Integrated static modelling and dynamic simulation framework for CO_2 storage capacity in upper Qishn Clastics, S1A reservoir, Yemen

Ayman Mutahar AlRassas (alrassas1989@gmail.com)
China University of Petroleum Huadong https://orcid.org/0000-0002-7539-1865
Hung Vo Thanh
Seoul National University
Shaoran Ren
China University of Petroleum Huadong
Renyuan Sun
China University of Petroleum Huadong
Nam Le Nguyen Hai
Ho Chi Minh City University of Technology: Truong Dai hoc Bach khoa Dai hoc Quoc gia Thanh pho Ho Chi Minh
Kang-Kun Lee
Seoul National University

Research Article

Keywords: Geological model, Uncertainty assessment, Carbon Capture & Storage, CO2 static & dynamic

Posted Date: June 2nd, 2021

DOI: https://doi.org/10.21203/rs.3.rs-503826/v1

Abstract

Carbon dioxide (CO_2) capture and storage (CCS) is presented as an alternative measure and promising approach to mitigate the large-scale anthropogenic CO_2 emission into the atmosphere. In this context, CO_2 sequestration into depleted oil reservoirs is a practical approach as it boosts the oil recovery and facilitates the permanent storing of CO_2 into the candidate sites. However, the estimation of CO_2 storage capacity in subsurfaces is a challenge to kick-start CCS worldwide. Thus, this paper proposes an integrated static and dynamic modeling framework to tackle the challenge of CO_2 storage capacity in a clastic reservoir, S1A filed, Masila basin, Yemen.

To achieve this work's ultimate goal, the geostatistical modeling was integrated with open-source code (MRST-CO2lab) for reducing the uncertainty assessment of CO_2 storage capacity. Also, there is a significant difference between static and dynamic CO_2 storage capacity. The static CO_2 storage capacity varies from 4.54 to 81.98 million tons, while the dynamic CO_2 simulation is estimated from 4.95 to 17.92 million tons. Based on the geological uncertainty assessment of three ranked realizations (P10, P50, P90), our work was found that the upper Qinshn sequence could store 15.64 Million tons without leakage. This result demonstrates that the potential of CO_2 utilization is not only in this specific reservoir, but the further CO_2 storage for the other clastics reservoirs is promising in the Masila Basin, Yemen.

1. Introduction

Geological carbon storage has been considered as a potential technology for slowing down CO_2 emissions to mitigate climate change (Bachu 2000). There are several sequestration projects in onshore and offshore around the world, including Sleipner in offshore Norway (Singh et al. 2010), Big Sky in Kevin Dome site, USA (Dai et al. 2014), Shenhua site in Ordos Basin, China (Nguyen et al. 2017a), onshore Salah in Algeria, Africa (Eiken et al. 2011). In Yemen, the oil and gas industry made a lot of impact on the environment. Especially CO_2 emission is increasing strongly in recent years. Thus, the potential of CO_2 storage in the petroleum field is necessary to explore for proposing a suitable plan for Carbon Capture Storage (CCS) in Yemen. The Masila Basin is the largest sedimentary basin in Yemen (Al-Areeq and Maky 2015). This basin contains more than 80% of the country's oil reserve. Therefore, the CO_2 utilization in these large oil fields is promising for Yemen to contribute to the emergency issue in the world, namely global warming and climate change.

In the early stage of a CCS project, the CO_2 storage capacity is one of the essential steps before moving to any decision making. In this vein, the 3D geological modeling techniques could provide a manner picture of storage sites. The understanding of reservoir capacity and heterogeneity would provide a clear vision about subsurface CO_2 injection purposes. However, reservoir modeling always faced the challenge of limitation and uncertainty geological data (Zhang et al. 2016; Vo Thanh et al. 2020). This issue leads to finding out suitable modeling methods to enhance the lithofacies and petrophysical properties that represent the subsurface concept (Thanh and Sugai 2021). Several modeling tools have been proposed

to construct the 3D geological facies, porosity, and permeability models. These tools consisted of sequential indicator simulation (SIS), object-based modeling (OBM), multiple-point geostatistics (MPS), assign value, and neural network.

Moreover, Albert et al. (1992) proposed the stochastic models of a deepwater reservoir considering Gaussian, SIS, and fractal simulation. Seifert and Jensen (2000) conducted the facies modeling of braided fluvial reservoirs using pixel and object-based modeling techniques. These scholars suggested that modeling method choosing is as important as selection model factors, as both can affect the estimation of pore volumes (Nguyen et al. 2017b). Regarding the porosity and permeability properties are commonly distributed using stochastic pixel-based methods while the modeled values are conditioned to a well dataset (Vo Thanh et al. 2019b). Several methods for continuous petrophysical property modeling were proposed to maintain the geostatistical information and correlation between primary and secondary parameters(Pyrcz and Deutsch 2014). For detail, Sequential Gaussian Simulation (SGS) is a popular tool usually adapted in geological modeling due to its ease and pliability to generate continuous porosity and permeability models(Emery and Peláez 2011). Furthermore, porosity is an additive reservoir parameter and typically reveals low variability. Thus, SGS is frequently the most suitable method to build porosity models. In order to distribute permeability in 3D models, two types of methods are commonly utilized in the modeling process (Nguyen et al. 2017a).

Firstly, porosity and permeability transform using correlation equations between porosity and permeability. Secondly, the simulation of permeability is additionally constrained by the modeled porosity to represent the spatial cross-correlation in the 3D model (Nguyen et al., 2017a). However, the accuracy of these methods depends on accurate models of cross-variograms that make the challenge for limitation datasets in reservoirs. (Nguyen et al., 2017a).

Furthermore, the evaluation of CO_2 storage needs to further consider dynamic flow in the subsurface. Static and dynamic CO_2 storage capacity should be estimated for candidate sites. Also, the dynamic simulation could be used for injection screening and risk analysis in CCS projects (Bérard et al. 2007; Benson and Cole 2008; Celia et al. 2015; Ren and Duncan 2019) Jin et al. (2012) explored different methods for estimation CO_2 storage in saline formation in the UK. These authors used the ECLIPSE reservoir simulator for their dynamic simulation to investigate the CO_2 migration for a future monitoring plan. Nghiem et al.(2009) used CMG-GEM for optimization residual and solubility trapping in saline aquifers.

Recently, open-source simulation code had great attention for the CCS community. MATLAB Reservoir Simulation Toolbox (MRST)-CO2lab open-source was developed by SINTEF for CO_2 storage modeling. This module could estimate CO_2 storage capacity for large-scale in the North Sea. Also, the developer spent more than 10 years testing and evaluating the efficiency of the MRST CO2-lab.

Halvor et al. (2016) proposed the simulation workflow for large-scale CO_2 storage using MRST-CO2lab in simple models. These scholars demonstrated the efficiency of MRST-CO2lab for the evaluation of

potential CO_2 storage on a large scale.

Based on the literature review mentioned above, this study would present the workflow for CO_2 storage capacity in one of the reservoirs in offshore Yemen. The synergy of the commercial package and open-source simulation was introduced in this work. To the author's knowledge, this study is firstly conducted for CO_2 storage in Yemen. The success story of this study will motivate oil and gas companies of Yemen to kick-start the CO_2 storage in petroleum fields. Briefly, our work would achieve the specific goals following:

- Evaluation of the static and dynamic CO_2 storage in Clastic reservoir in Yemen
- Utilizing the open-source code for reservoir simulation CO_2 trapping
- Proposing the workflow for future CCS projects in Yemen

2. Geological Background

Masila Basin is an onshore basin located in the east part of the Hadramout region, Yemen, and is considered the most productive basins (Lashin et al. 2016). Block-14 is situated in the Masila basin, and it consists of more than 18 oilfields (Al-Areeq and Maky 2015). Block-14 is an irregular-shaped concession falling within a rectangle that is 1250 km2. Sunah oilfield is located in the northeast of Block-14. It occupies the central west of the Masila basin between longitudes 49° 00' ' E and 48° 60' E and latitudes 15° 50‘ N and 15° 90' N. Sunah oilfield consists of eight reservoirs. Upper Qishn Clastics in Sunah oilfield consists of four structural, namely S1A, S1C, S2, and S3. However, S1A sandstone is the target reservoir of this study with an estimated STOIIP of 76 MMSTB. (Fig. 1) represents the map location of the S1A reservoir, Sunah oilfield, Masila basin, Yemen.

As the sequence of the Aden’s gulf and the red sea rifting during the Tertiary age, the Masila basin was subjected to several faults trending North West-South East, resulted from the structural development, which extended in WNW-ESE direction. The formation of the Masila basin was created by rifting during the Late Jurassic and Early Cretaceous. The upper Qishn sandstones of the Qishn Formation have been Stratigraphically subdivided into three informal units: an upper S1, a middle S2, and a bottom S3. S1 refers to the first sandstone encountered below the Qishn Carbonates Member, followed by the S2 and S3. The S1 is subdivided into S1A, S1B, and S1C, based on the presence or absence of non-reservoir (carbonate and shale) lithologies. The Sunah Field is placed on a faulted basement high in the northwest corner of the Masila Block. The S1A formation consists of tidally and longshore influenced shelf sands and varies in thickness from 25–40 feet. The S1A reservoir quality sand appears to be continuous through at the Sunah oilfield. The net pay of the S1A varies in thickness from 10–35 ft with porosities between 18 – 27%. Four main faults crosscut the S1A shelf sands. These four faults strike east-west and dip to the south. This has resulted in the formation of four structural pools on the footwall or northern side of the faults. The Sunah S1A structural pools are isolated from the NE Sunah, Hemiar, and Camaal S1A structural pools, by water-filled structural low or spill point approximately-2700ft ss (Sub-sea).

Transmissive fault barriers separate the four Sunah structural. (Fig. 2) illustrates the lithological stratigraphy of S1A reservoir, Sunah oilfield, Masila basin, Yemen.

3. Material And Method

3.1.Material

The databases of this study consist of check-shot, geological reports, lithological information, deviation surveys, total vertical depth (TVD), and wireline logs [consisting of spontaneous potential (SP), caliper (CAL), acoustic impedance (AC), and gamma-ray (GR)] from 74 drilled wells in S1A reservoir, Sunah oilfield, Masila basin. These datasets were employed to depict the internal subsurface structure of the S1A reservoir and petrophysical heterogeneity of the S1A reservoir. These datasets were integrated into Petrel software and utilized to construct three-dimensional models, including structural model, facies model, petrophysical model, as well as determining the pore volume.

3.2 Methodology

This paper investigates the effect of a 3D geological model and dynamic simulation to evaluate the potential of CO_2 storage capacity in the S1A oilfield. (Fig.3) depicts the entire workflow about geological modeling and reservoir simulation for this study.

3.2.1. Geological Modeling

Three-dimensional geological modeling was conducted employing Petrel software to evaluate the structural attributes, facies depositions, and petrophysical properties, including porosity, permeability, and water saturation. The following subsection will explain in detail the modeling procedure of this paper.

3.2.1.1 Structural modeling

The structural model is considered the initial stage to construct the static model (Abdel-Fattah et al. 2018). Virtually, the structure model consists of fault modeling, gridding, and horizons (Rassas et al. 2020). All the processes mentioned were conducted sequentially to construct the structural model of the S1A reservoir. The initial stage of building a structural model was to identify the structural faults based on the well logs interpretations of S1A formation units. Fault polygon was employed to generate the fault surfaces using petrel tools for all curving faults, vertical faults, diagonal faults, as well as faults with various geometrical structures, all corresponding to their polygon. Fault polygons with diverse stratification planes were used to identify the initial surface. Thereafter, the fault section was modified to adjust the fault section correctly. After that, the structural model's skeleton was created by integrating 3D fault surfaces with horizons of the S1A reservoir. (Fig.4) presents the structural model of the S1A reservoir.

3.2.1.2. Lithofacies modeling

The upper Qishn sandstones of the Qishn Formation have been stratigraphically subdivided into three informal units: an upper S1, a middle S2, and a bottom S3. In detail, S1 refers to the first sandstone encountered below the Qishn Carbonates Member, followed by the S2 and S3. Furthermore, the S1 unit is subdivided into S1A, S1B, and S1C, based on the presence or absence of non-reservoir (carbonate and shale) lithologies. The S1A lithofacies model was developed based on the analysis of the lithofacies characteristics of sedimentary deposits provided in well logs. Typically, the facies model adapts various facies techniques to populate the discrete facies model, including object-modeling (OM), Indicator kriging (IK), and assigned value (AV). However, the facies model in the S1A reservoir was simulated employing the Simulation Indicator Sequential (SIS) technique.

3.1.2.3. Petrophysical property modeling

The spatial distribution of reservoir properties within the geological grid is crucial to investigate the distribution of the petrophysical properties (Abdel-Fattah et al. 2018; Islam et al. 2021). In this study, the petrophysical properties, including porosity, permeability, and water saturation of the S1A reservoir, were determined from well-logging data by employing Petrel software. The well-based petrophysical properties were upscaled and distributed laterally, employing the Sequential Gaussian Simulation (SGS) technique in association with the lithofacies model to identify the reservoir heterogeneities at various scales. SGS is the most commonly used geostatistical approach to generate stochastic random spatial fields with continuous parameters for the petrophysical modeling process (Pyrcz and Deutsch 2014)

3.2.1 Reservoir Simulation

The previous studies mainly were applied to commercial reservoir simulators such as ECLIPSE, CMG for CO_2 simulation in field scale. However, this study used the MRST_CO2lab module for investigating dynamic CO_2 storage in the Sunah field.

The reservoir simulation results are a more detailed inventory that accounts for six distinct CO_2 categories: To begin with, residual (traps) refers to CO_2 that has remained stuck inside a structural pit. Second, there's residual CO_2, which is CO_2 that hasn't been caught by any structural traps. Third, residual (plume) considers the portion of the CO_2 migration that would be left outside of any structural traps. Next, movable (traps) refers to mobile CO_2 volume that is actually trapped within a residual trap and is free to move upward if the caprock is broken. The movable (plume) is the portion of the CO_2 plume that is free to migrate upward or can be displaced by any imbibing brine (outside of any structural traps). Finally, the CO_2 leaked is the volume of CO_2 that has migrated out of the domain through its lateral boundaries (Gasda et al. 2013; Møll et al. 2016a; Allen et al. 2017).

The Vertical-Equilibrium (VE) model was used for simulating CO_2 trapping in the subsurface. The primary assumption in a vertical equilibrium model is allowing the vertical distribution of fluid phases to be calculated using analytical expressions (Møll et al. 2016b). The flow equations can then be integrated

vertically to obtain a simplified model. This is a common method used in many other branches of physics, such as explaining water waves, creep flow, and so on (Møll et al. 2016b)

The effect of vertical direction decreases the number of field dimensions. Thus, this leads to reducing the coupling between pressure and fluid transport and improving the problem's characteristic time constants (Møll et al. 2016b).

Therefore, the VE models could reduce computation time when compared with 3D conventional simulators.

In our work, the ranking geological models (P10, P50, P90) were used for uncertainties analysis of static and dynamic CO_2 storage. The other input reservoir simulation parameters are expressed in detail in (**Table.1**).

Table 1 Model input parameters used in this study

Parameter	Unit	Value
Residual water saturation (Srw)		0.27
Residual CO_2 saturation (Src)		0.2
Pressure reference (P_ref)	MPa	20
Temperature (t_ref)	K	94+273.15
Rock compressibility (c_rock)	1/barsa	4.35e-5
Capillary entry pressure	KPa	5
Brine viscosity (muw)	Pascal*second	8e-4
CO_2 viscosity	Pascal*second	CO_2.mu(p_ref, t_ref)
Injection rate	m^3/day	5000-7000

4. Result And Discussion

4.1.Petrophysical modeling results

The initial stage for constructing 3D reservoir models is building the structural modeling, which relies on well-logs interpretations. The goal of 3D structural modeling is mainly to obtain a 3D interpretation and understanding of the geological structure. Structural model construction relies on main components, including faults patterns and horizons of oil and gas accumulation (Avseth et al. 2005). The structural model of the S1A reservoir, Sunah oilfield, is defined by the horizon and fault framework and creates the geometrical data for constructing the 3D grid. S1A oilfield is a sandstone reservoir interbedded with slight limestone, mudstone, and siltstone. Well correlation for S1A reservoir was conducted for 74 wells to present the significant variations in thickness and petrophysical properties in the four zones of the S1A reservoir. The S1A lithological units were subdivided into three units: upper shore, mid-shore, and low shore. The correlation was conducted by employing various logs, including Spontaneous potential (SP), Gamma Ray (GR), Resistivity (RT), and Acoustic impedance (AC). The S1A reservoir consists of four

horizons, namely S1A-F1, S1A-F2, S1A-F3, S1A-F4, and S1B, which is divided sequentially from the tops to the bottom. Fig.5 presents the S1A reservoir result of surface modeling A, B, C, and D**.** The mapped horizons of the S1A reservoir indicated that formation units are laterally extended within the model area and influenced by the normal faults that were interpreted. The S1A shelf sands are crosscut by four main normal faults A-D. These four faults strike East-West and dip to the south. This has resulted in the formation of four S1A structural pools, A-D, on the footwall or northern side of the faults. Additionally, other faults affect trends to NW-SE influence the area of target study.

On the other hand, the S1A structural pools are isolated from other oilfields in the Masila Basin, including the North-East Sunah, Hemiar, and Camaal S1A structural pools, by water-filled structural low or spill point at approximately -2700 ft ss. The S1A structural pools are sealed by the overlying red Shale and Qishn Carbonate formations. The four Sunah structural pools, A–D, are separated by transmissive fault barriers. These “leaky” fault barriers indicate that the four Sunah pools may carry the exact initial reservoir pressure and the same initial oil/water contact. The lowest known oil (LKO) in the “A” pool is observed in the Sunah-41Z well at -2616 ft SS. The “B” pool has an LKO of –2640 ft ss observed in the Sunah-40 well. A LKO of –2643 ft SS has been established in the “C” pool by the Sunah-29 well. The lowest known oil (LKO) in the “D” pool is observed in the Sunah-43Z well at -2651 ft SS. (Fig.6) presents the S1A structural pools.

4.1.1. Facies Model

The lithofacies model has a significant contribution in controlling the distribution of petrophysical properties. The lithofacies model can be conducted by utilizing an appropriate technique, including stochastic and deterministic, which provides facilities to construct 3D spatial distributions of property models that can acquire from well datasets (Ali et al. 2020). The process of generating the facies log from the existing wells was the initial step for developing the facies model of the S1A reservoir (Abdel-Fattah et al. 2018; Rassas et al. 2020). However, before constructing the facies model, the lithofacies logs were created and upscaled to the grid model of the S1A reservoir. The facies model of the S1A reservoir was divided into four zones, namely S1A-F1, S1A-F2, S1A-F3, and S1A-F4. The S1A lithological units were subdivided into three units: upper shore, mid-shore, and low shore, with different proportions of 53.3%, 28.67%, and 18.03%, respectively.

Moreover, the S1A is a sandstone reservoir interbedded with slight limestone, mudstone, and siltstone. Furthermore, facies models are adapted to various facies techniques to populate the discrete facies model; however, the Simulation of Sequential Indicator (SIS) approach was employed to simulate the lithofacies model of S1A reservoir by a stochastic approach. A stochastic approach can integrate the volume fraction and variograms. Virtually, the stochastic approach is considered suitable with minimal data, specifically when the sand body is uncertain. Moreover, it facilitates the modeling of the sand body environment in which the facies volume ratio differs laterally and vertically. (Fig.7) presents the results of the S1A reservoir lithofacies model.

4.1.2. Porosity Model

Evaluation of hydrocarbons trapped in the oil reservoir is obtained by determining the reservoir's porosity (Agyare Godwill and Waburoko 2016; Rassas et al. 2020). The porosity model was constructed based on well-logs interpretations of the S1A reservoir. The well logs were scaled up utilizing the average arithmetic approach. Moreover, a Sequential Gaussian Simulation (SGS) algorithm was employed to distribute the porosity model within the S1A reservoir. Furthermore, the porosity value of the S1A reservoir ranges from 0% to 27%, with an average distribution of 22%. The lowest porosity values were found in the northern and eastern regions, while the highest values are situated in the central and northeastern areas. Approximately 60% of porosity values range between 0.10 to 0.20, while 40% range from 0.05 to 0.1. Vertically, a reversal relation between porosity values and depth was increasing. Overall, the result indicates that the porosity value within the S1A reservoir is a good sandstone reservoir. (Fig.8) represents the result of a porosity model in the S1A reservoir.

4.1.3.Permeability Model

The term permeability refers to the fluid movement's ability within the porous reservoir media (Agyare Godwill and Waburoko 2016; Rassas et al. 2020). Virtually, permeability plays a substantial role in determining the fluid flow trends and fluid flow rate. The permeability model was developed based on well-logs interpretations of the S1A reservoir. The well logs were scaled up utilizing the average arithmetic method. The (SGS) approach was utilized to distribute the permeability model within the S1A reservoir. The Permeability value ranges from 1 to 1000 md with an average distribution of 800 md within the S1A reservoir. The Permeability values centralized in with 2550 md. Approximately 90% of Permeability values range between 200 to 800 md, while 20% range more or less. Overall, the results indicate that the permeability value within the S1A reservoir is a good sandstone reservoir. (Fig.9) presents the permeability model of the S1A reservoir.

4.1.4 Water Saturation model

The ratio of oil, water, and gas in the pore media is known as the saturation distribution (Ali et al. 2020; Rassas et al. 2020; Islam et al. 2021). Saturation is a crucial form for specifying water areas with high potential. The average arithmetic method was employed to scale up the well logs. The (SGS) approach was used to distribute the water saturation model within the S1A reservoir. The water saturation value ranges from 0.1 to 0.7, with an average distribution of 0.75 within the S1A reservoir. The lowest water saturation values were found in the center, while the highest values were found in the boundary of the reservoir. Roughly, 80% of water saturation values range between 0.50 to 0.80, while 20% of them range from 0.1 to 0.3. Vertically, a proportional relation between water saturation values and depth increasing. (Fig.10) presented the result of water saturation within the S1A reservoir.

4.2. Geological uncertainty of petrophysical models

The uncertainties still exist in the model of the S1A reservoirs. Firstly, the structural model is still unconfident due to seismic interpretation from a geophysical aspect. Secondly, the facies model is not studying from a depositional conceptual model. The intermediate conceptual model has been referred to

as for assumption of direction, location, and size of geological features distribution. Also, well log up-scale, and grid up-scaling themselves lead to model uncertainty, particularly Pore Volume. The Pore Volume is extremely important for static CO_2 storage capacity in the subsurface.

On the other hand, the geological uncertainties could provide the uncertainties range (P10, P50, P90) for the porosity and permeability model. These plausible geological realizations are considered as rank models for dynamic CO_2 storage capacity.

The uncertainty assessment was conducted from a geological package. In this paper, the global seed number is considered as the main parameter for finding the uncertainty values of Pore Volume. Also, the global seed number will be assigned to changed 100 porosity and permeability models. That means each pore volume calculation led to a change in each porosity and permeability. Then, the global seed number from P10, P50, and P90 pore volume was adapted as the global seed number for porosity and permeability models.

The Monte Carlo Simulation with Latin Hyper Sampling was used to determine the probability distribution of reservoir pore volume. The P10, P50, P90 pore volume was used for risk assessment of static CO_2 storage capacity. (Fig.11) represents the result of uncertainty analysis of pore volume in the S1A reservoir.

Furthermore, the ranked porosity and permeability model was also obtained from the geological uncertainties process. (Fig.12) illustrates the three realizations (P10, P50, P90) of porosity and permeability models. These 3D images showed the significant difference between three realizations (porosity and permeability) that represents the overall geological uncertainty in the reservoir.

4.3 Theoretical CO_2 storage capacity

The static CO_2 storage capacity evaluates from petrophysical data of the potential candidate sites. There are many ways for determining the potential of CO_2 storage capacity for structural trapping, capillary trapping, and dissolution trapping (Bradshaw et al. 2007; Zhong and Carr 2019)

This paper emphasizes on static CO_2 storage capacity by using the equation below:

$$M_{co2} = A \times \mathrm{h} \times \phi \times (1 - S_{wiir}) \times \mathrm{B} \times \rho_{co2} \times \mathrm{E} \qquad \text{(Eq.1)}$$

where M_{CO2} is estimated CO_2 storage capacity (Mt), *A* is trap area (m^2), *h* is the average thickness (m), ϕ is the porosity of storage site (%), S_{wiir} is known as irreducible water saturation (%), B knows as a formation volume factor in the storage site (m^3/m^3), ρ_{CO2} is the CO_2 density (kg/m^3), and E is the capacity coefficient (IEA GHG 2008; Vo Thanh et al. 2019a).

However, the trap area, porosity, and thickness can be included in many uncertainties in the geological modeling process. Therefore, we consider the sum of grid pore volumes ($V_{pv}=\sum iAi\times hi\times \phi i$) to swap $A\times h\times \phi$ (Vo Thanh et al., 2019a). The new formula can be replaced as follows:

$$M_{CO2} = V_{pv} \times (1 - S_{wiir}) \times B \times \rho_{CO2} \times E \qquad \text{(Eq.2)}$$

where Vpv is the pore volume of a reservoir (m^3)

Thus, the static CO_2 storage capacity can be computed by considering Equation (2) and (Table 2).

Table 2 Uncertainty assessment for theoretical storage capacity in S1A reservoir

Parameters	Symbol	Unit	P10	P50	P90
Pore volume	V_{pv}	Mm^3	60.24	78.83	97.51
Irreducible water saturation	S_{wiir}	%	0.34	0.24	0.11
Formation volume factor	B	Bbl/STB	1.35	1.35	1.35
Average CO_2 density	ρ_{CO2}	Kg/m^3	769	769	769
Capacity coefficient	E	%	0.11	0.51	0.91
CO_2 storage capacity	M_{CO2}	Mt	4.54	31.72	81.98

(Table 2) illustrates the three probability of static CO_2 storage in the S1A reservoir. The amount of P90 CO_2 storage achieves the highest values compared with P10 and P50 CO_2 storage capacity. There has been a strong increase of CO_2 storage amount from 4.54 Mt P10 to just over 31.71 Mt P50. Overall, it is clear that the least likely, P10, storage capacity was 4.54 million tons, and the most likely, P90, storage capacity was 81.98 million tons

In this context, we consider that this sandstone reservoir is potential CO_2 storage. Also, this evaluation is just for structural/stratigraphic trapping. The dynamic CO_2 simulation will further investigate the other

type of CO_2 trapping using MRST_CO2lab. This open-source code was used to simulate the CO_2 trapping mechanism in the Sunah field. The next section will elaborate on the CO_2 behavior inside the reservoir.

4.4 Dynamic CO2 storage capacity

The results of the dynamic CO_2 storage capacity were applied for three realizations (P10, P50, P90). The reservoir properties and injection rate were considered as the sensitivity impact of dynamic CO_2 storage. MRST-VE open-source MATLAB code could perform the quick CO_2 injection process in the subsurface. Thus, this source could be considered for this study. All simulation scenarios will be conducted in 10 years of injection and 90 post-injection periods. The grid simulation cell with 188×144×20 (391040 grid cells). A large number of grid cells could produce a reliable simulation in the subsurface.

The injection rate is an important parameter for dynamic storage capacity. The injection rate will monitor the balance between buoyancy and CO_2 horizontal spread. Also, the increasing injection rate will lead to improved sweep efficiency for well injection operation. However, the disadvantage of a large injection rate is CO_2 leakage risk.

At the first step of the MRST-VE module, the 3D grid cell will be converted approximately to a 2D form shape. (Fig.13) illustrates the result of the processing grid cell for the S1A field to conduct the dynamic storage assessment.

(Fig.14) represents the CO_2 saturation migration in three ranked geological realizations. The visualization of this CO_2 saturation indicated that the injection rate improved the CO_2 sweep efficiency in the storage sites. Besides, the large injection rate could be more suitable in the storage sites that have long horizontal sides. Also, (Fig.15) gives an idea about the petrophysical distribution effect on CO_2 migration. Although, the increasing injection rate was improved sweep efficiency. However, the diversity of reservoir heterogeneity was strongly affected by changing the morphology of the CO_2 plume in the S1A reservoir.

Also, the simulation results will suggest the CO_2 leakage potential according to the injection rate analysis. (Fig.15) represents the comparison of P10, P50, and P90 realizations according to the percentage of different types of CO_2 trapping with sensitivity injection rate.

This bar chart represents the amount of CO_2 trapping in P10, P50, and P90 geological realizations. It also highlighted the potential CO_2 leakage in three realizations. The green column illustrated the percentage of CO_2 leakage with an injection rate varying from 5000 m^3/day to 7000 m^3/day.

There were 5 types of CO_2 trapping obtained after 10-year injection and 90 years post-injection period in (Fig.15).

In terms of 5000 m^3/day, the amount of residual CO_2 trapping increased light from 32 % to 36%. Regarding the residual (traps) is stable in three realizations. In terms of residual (plume), the percentage

of CO_2 trapping has slightly decreased from 23% to 21%. Similarity with residual (traps), the movable (traps) of P90 realization slightly decreased 1% compared with P10 and P50 realizations.

Regarding the injection rate with 6000 m^3/day, the five type trapping percentage is slightly increasing or decreasing. However, the CO_2 will be leaked in three realizations if the injector operates with an injection rate equal to 6000 m^3/day.

Moreover, the movable (plume) achieved the highest amount with the largest injection rate (7000 m^3/day). The higher injection rate will supply a large amount in the injection period. This mechanism contributes to improving CO_2 sweep efficiency in storage reservoirs. Even so, the CO_2 leakage is strongly increased with the largest injection for three realizations.

Overall, the P50 geological realization with the lowest injection rate (5000 m^3/day) was the best strategy for decision-making under geological uncertainty. Also, the dynamic CO_2 storage capacity under geological uncertainty would provide a better plan for future development plans about geo-sequestration in the S1A reservoir.

Finally, the comparison between static and dynamic CO_2 storage would be considered. This step will answer the question of why dynamic CO_2 storage under geological uncertainties is important in CCS projects. (Fig.16) depicts the difference between static and dynamic CO_2 storage capacity in the upper Qishn Clastics.

The bar chart represents how much static and dynamic CO_2 storage capacity in P10, P50, and P90 realization. There was a slight difference between static and dynamic CO_2 storage in P10 realization. A difference about half was evidence in static and dynamic in P50 realization where P50 static is 15.65 Mt and P50 dynamic is 31.72 Mt. Similarly, more static CO_2 is stored than dynamic CO_2 trapping (approximately 81.98 and 17.52).

The main reason for the difference between static and dynamic is the efficient storage factor in the static calculation. Also, the dynamic CO_2 storage capacity is considered CO_2 leakage during the simulation process. Therefore, the results will be different in terms of static and dynamic CO_2 storage.

In addition, this study demonstrated the important role of CO_2 storage capacity under geological uncertainty. The CO_2 storage capacity will include a lot of uncertainty factors. Our work emphasizes the role of petrophysical modeling uncertainties from static to dynamic CO_2 storage capacity. It could provide the template for future development about Carbon Capture Storage in Yemen.

5. Conclusion

The petrophysical properties of geological models play a significant role in determining the static and dynamic model of CO_2 storage capacities. The construction of accurate 3D geological models facilitates

the distribution of petrophysical models. A robust and reliable 3D geological model streamlines the comprehension of CO_2/oil flow during the improved oil production and selecting the suitable storage site of CO_2. In conclusion, the critical points of this could be remarked as follows:

- Well-logs interpretations were used to evaluate the lithofacies and petrophysical properties of the S1A reservoir.
- Facies model of the S1A reservoir was divided into four formations, namely S1A-F1, S1A-F2, S1A-F3, and S1A-F4. Three lithological units exist in the S1A reservoir: upper shore, mid-shore, and low shore, with various proportions of 53.3%, 28.67%, and 18.03%, respectively. Moreover, the S1A oilfield is a sandstone reservoir interbedded with slight limestone, mudstone, and siltstone.
- A sequential Gaussian Simulation (SGS) algorithm was employed to distribute the petrophysical property model within the S1A reservoir. The porosity range between 0% -27%, with an average distribution of 22%, while the permeability range between 1 to 1000 md, with an average distribution of 800 md. The water saturation was ranged from 0.1 to 0.7, with an average distribution of 0.75.
- Based on the static estimation, the maximum amount of CO_2 storage capacity in the Upper Qishn Clastics reservoir is 81.98 million tons.
- The dynamic CO_2 simulation explored that the reservoir could safely store a maximum of 15.64 million tons.
- Geological uncertainty is a necessary step for both static and dynamic CO_2 storage to reduce the risk.
- The future work will adapt the developed modeling workflow for other candidate storage sites in Masila Basin, Yemen.

Declarations

Conflicts of interest: The authors declare no conflict of interest.

References

Abdel-Fattah MI, Metwalli FI, Mesilhi ESI (2018) Static reservoir modeling of the Bahariya reservoirs for the oilfields development in South Umbarka area, Western Desert, Egypt. J African Earth Sci 138:1–13. https://doi.org/10.1016/j.jafrearsci.2017.11.002

Agyare Godwill P, Waburoko J (2016) Application of 3D Reservoir Modeling on Zao 21 Oil Block of Zilaitun Oil Field. J Pet Environ Biotechnol 07:1–8. https://doi.org/10.4172/2157-7463.1000262

Al-Areeq NM, Maky AF (2015) Organic geochemical characteristics of crude oils and oil-source rock correlation in the Sunah oilfield, Masila Region, Eastern Yemen. Mar Pet Geol 63:17–27. https://doi.org/10.1016/j.marpetgeo.2015.01.017

Alabert FG, Aquitaine E, Modot V, Nancy M De (1992) Stochastic Models of Reservoir Heterogeneity : Impact on Connectivity and Average Permeabilities

Ali M, Abdelmaksoud A, Essa MA, et al (2020) 3D Structural , Facies and Petrophysical Modeling of C Member of Six Hills Formation , Komombo Basin , Upper Egypt. Nat Resour Res 29:2575–2597. https://doi.org/10.1007/s11053-019-09583-5

Allen R, Nilsen HM, Andersen O, Lie K-A (2017) On obtaining optimal well rates and placement for CO2 storage. Comput Geosci 21:1403–1422. https://doi.org/10.1007/s10596-017-9631-6

Avseth P, Mukerji T, Mavko G (2005) Quantitative Seismic Interpretation. Quant Seism Interpret. https://doi.org/10.1017/cbo9780511600074

Bachu S (2000) Sequestration of CO2 in geological media: Criteria and approach for site selection in response to climate change. Energy Convers Manag 41:953–970. https://doi.org/10.1016/S0196-8904(99)00149-1

Benson SM, Cole DR (2008) CO2 sequestration in deep sedimentary formations. Elements 4:325–331. https://doi.org/10.2113/gselements.4.5.325

Bérard T, Jammes L, Lecampion B, et al (2007) CO2 storage geomechanics for performance and risk management. In: Offshore Europe Conference - Proceedings. Aberdeen, Scotland, U.K., 4–7 September 2007, pp 189–196

Bradshaw J, Bachu S, Bonijoly D, et al (2007) CO2 storage capacity estimation: Issues and development of standards. Int J Greenh Gas Control 1:62–68. https://doi.org/10.1016/S1750-5836(07)00027-8

Celia MA, Bachu S, Nordbotten JM, Bandilla KW (2015) Status of CO2 storage in deep saline aquifers with emphasis on modeling approaches and practical simulations. Water Resour Res 51:6846–6892. https://doi.org/10.1002/2015WR017609

Dai Z, Stauffer PH, Carey JW, et al (2014) Pre-site characterization risk analysis for commercial-scale carbon sequestration. Environ Sci Technol 48:3908–3915. https://doi.org/10.1021/es405468p

Eiken O, Ringrose P, Hermanrud C, et al (2011) Lessons Learned from 14 years of CCS Operations: Sleipner, In Salah and Snøhvit. Energy Procedia 4:5541–5548. https://doi.org/10.1016/j.egypro.2011.02.541

Emery X, Peláez M (2011) Assessing the accuracy of sequential Gaussian simulation and cosimulation. Comput Geosci 15:673–689. https://doi.org/10.1007/s10596-011-9235-5

Gasda SE, Nilsen HM, Dahle HK (2013) Impact of structural heterogeneity on upscaled models for large-scale CO2migration and trapping in saline aquifers. Adv Water Resour 62:520–532. https://doi.org/10.1016/j.advwatres.2013.05.003

Halvor KL, Nilsen M, Andersen O, Møyner O (2016) A simulation workflow for large-scale CO 2 storage in the Norwegian North Sea. Comput Geosci 607–622. https://doi.org/10.1007/s10596-015-9487-6

IEA GHG I (2008) Aquifer Storage-Development Issues

Islam A, Yunsi M, Qadri SMT, et al (2021) Three-Dimensional Structural and Petrophysical Modeling for Reservoir Characterization of the Mangahewa Formation , Pohokura Gas-Condensate Field , Taranaki Basin , New Zealand. Nat Resour Res 30:371–394. https://doi.org/10.1007/s11053-020-09744-x

Jin M, Pickup G, Mackay E, et al (2012) Static and Dynamic Estimates of CO2-Storage Capacity in Two Saline Formations in the UK. SPE J 17:1108–1118. https://doi.org/10.2118/131609-PA

Lashin A, Marta E Bin, Khamis M (2016) Characterization of the Qishn sandstone reservoir, Masila Basin-Yemen, using an integrated petrophysical and seismic structural approach. J African Earth Sci 115:121–142. https://doi.org/10.1016/j.jafrearsci.2015.11.026

Møll H, Lie NK, Andersen O (2016a) Robust simulation of sharp-interface models for fast estimation of CO 2 trapping capacity in large-scale. 93–113. https://doi.org/10.1007/s10596-015-9549-9

Møll H, Lie NK, Andersen O (2016b) Fully-implicit simulation of vertical-equilibrium models. 49–67. https://doi.org/10.1007/s10596-015-9547-y

Nghiem L, Yang C, Shrivatava V, et al (2009) Optimization of Residual Gas and Solubility Trapping for CO 2 Storage in Saline Aquifers. Soc Pet Eng 1–9. https://doi.org/10.1016/j.egypro.2009.02.079

Nguyen MC, Zhang X, Wei N, et al (2017a) An object-based modeling and sensitivity analysis study in support of CO2 storage in deep saline aquifers at the Shenhua site, Ordos Basin. Geomech Geophys Geo-Energy Geo-Resources 3:293–314. https://doi.org/10.1007/s40948-017-0063-5

Nguyen MC, Zhang Y, Li J, et al (2017b) A Geostatistical Study in Support of CO2Storage in Deep Saline Aquifers of the Shenhua CCS Project, Ordos Basin, China. Energy Procedia 114:5826–5835. https://doi.org/10.1016/j.egypro.2017.03.1720

Pyrcz MJ, Deutsch C V. (2014) Geostastistical Reservoir Modeling. Oxford University Press, Oxford

Rassas A Al, Ren S, Sun R, et al (2020) Application of 3D Reservoir Geological Model on Es1 Formation , Block Nv32 , Shenvsi Oilfield , China. Open J Yangtze Gas Oil 54–72. https://doi.org/10.4236/ojogas.2020.52006

Ren B, Duncan IJ (2019) Reservoir simulation of carbon storage associated with CO 2 EOR in residual oil zones, San Andres formation of West Texas, Permian Basin, USA. Energy 167:391–401. https://doi.org/10.1016/j.energy.2018.11.007

Seifert D, Jensen JL (2000) Object and pixel-based reservoir modeling of a braided fluvial reservoir. Math Geol 32:581–603. https://doi.org/10.1023/A:1007562221431

Singh V, Asa S, Cavanagh A, et al (2010) Reservoir Modeling of CO 2 Plume Behavior Calibrated Against Monitoring Data From Sleipner , Norway. In: SPE Annual Technical Conference and Exhibition. Florence, Italy, 19–22 September 2010

Thanh HV, Sugai Y (2021) Integrated modelling framework for enhancement history matching in fluvial channel sandstone reservoirs. Upstream Oil Gas Technol 6:100027. https://doi.org/10.1016/j.upstre.2020.100027

Vo Thanh H, Sugai Y, Nguele R, Sasaki K (2020) Robust optimization of CO2 sequestration through a water alternating gas process under geological uncertainties in Cuu Long Basin, Vietnam. J Nat Gas Sci Eng 76:103208. https://doi.org/10.1016/j.jngse.2020.103208

Vo Thanh H, Sugai Y, Nguele R, Sasaki K (2019a) Integrated work flow in 3D geological model construction for evaluation of CO 2 storage capacity of a fractured basement reservoir in Cuu Long Basin , Vietnam. Int J Greenh Gas Control 90:102826. https://doi.org/10.1016/j.ijggc.2019.102826

Vo Thanh H, Sugai Y, Sasaki K (2019b) Impact of a new geological modelling method on the enhancement of the CO2 storage assessment of E sequence of Nam Vang field, offshore Vietnam. Energy Sources, Part A Recover Util Environ Eff. https://doi.org/10.1080/15567036.2019.1604865

Zhang L, Li X, Ren B, et al (2016) CO2 storage potential and trapping mechanisms in the H-59 block of Jilin oilfield China. Int J Greenh Gas Control 49:267–280. https://doi.org/10.1016/j.ijggc.2016.03.013

Zhong Z, Carr TR (2019) Geostatistical 3D geological model construction to estimate the capacity of commercial scale injection and storage of CO2 in Jacksonburg-Stringtown oil field, West Virginia, USA. nternational J Greenh Gas Control 80:61–75. https://doi.org/10.1016/j.ijggc.2018.10.011

Figures

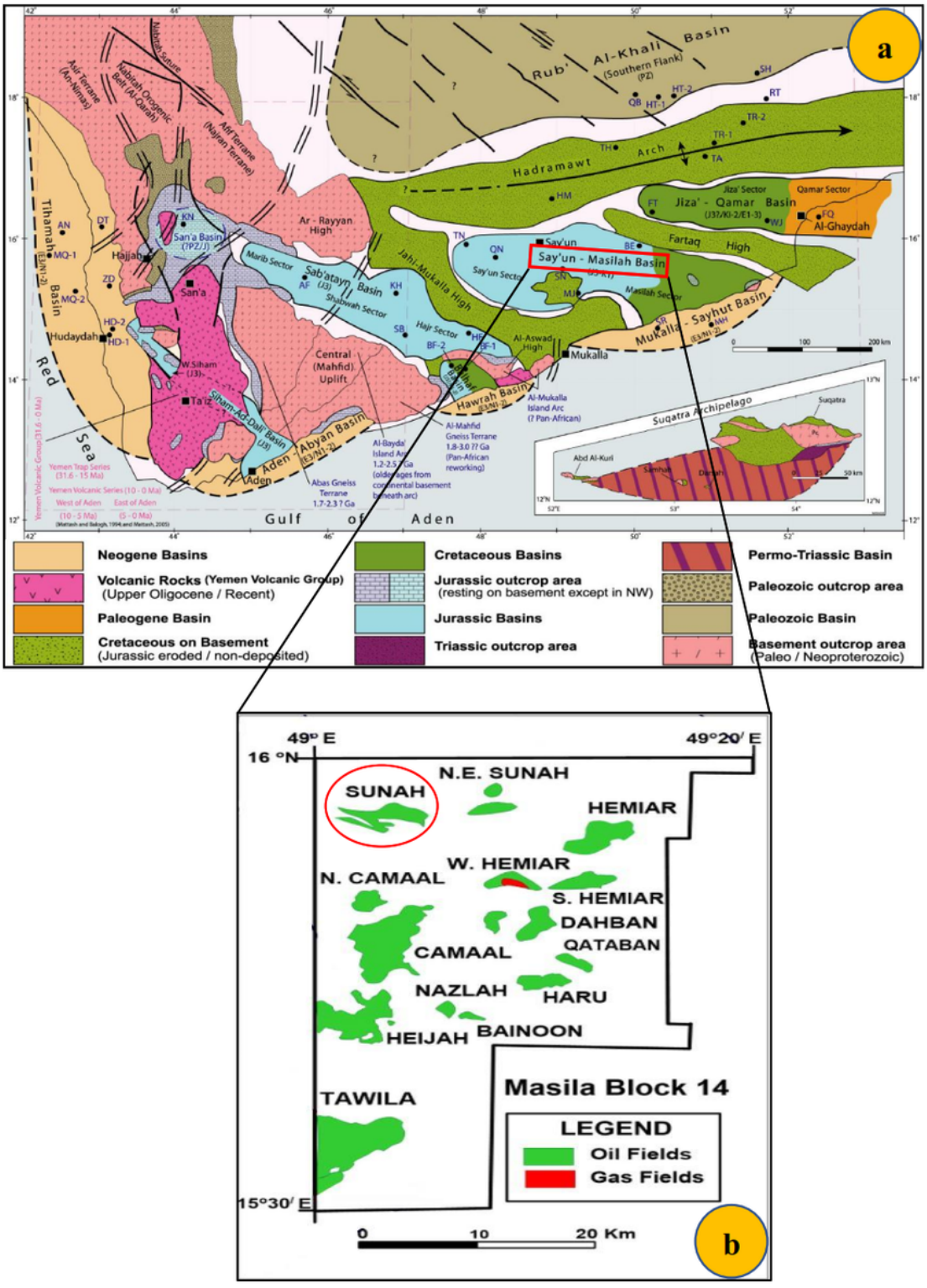

Figure 1

Study area. (a) Sedimentary basins of Yemen. (b)S1A reservoir, Sunah oilfield, Masila basin, Yemen

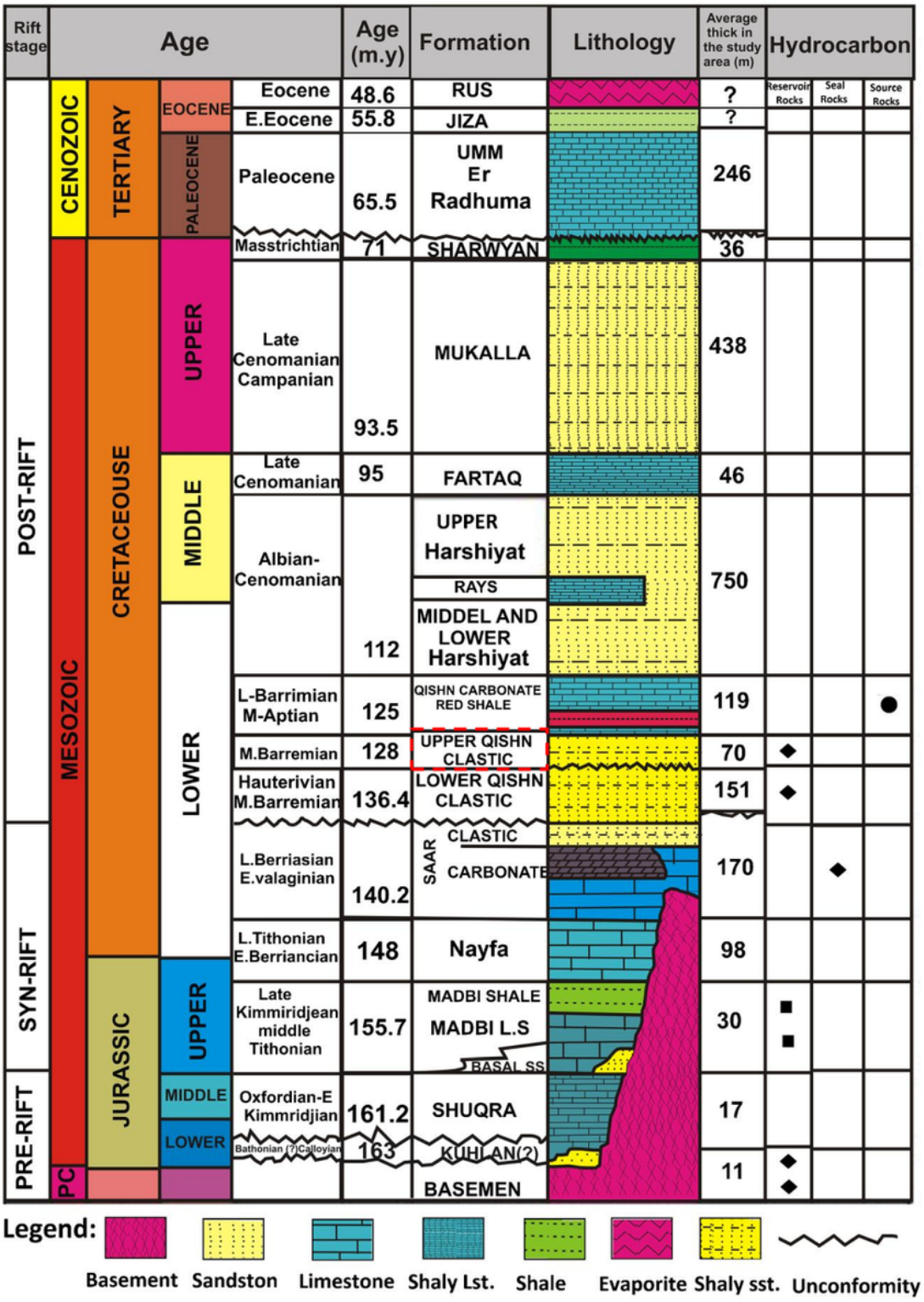

Figure 2

General stratigraphy of S1A reservoir, Sunah oilfield, Masila basin. The red box indicates the study area.

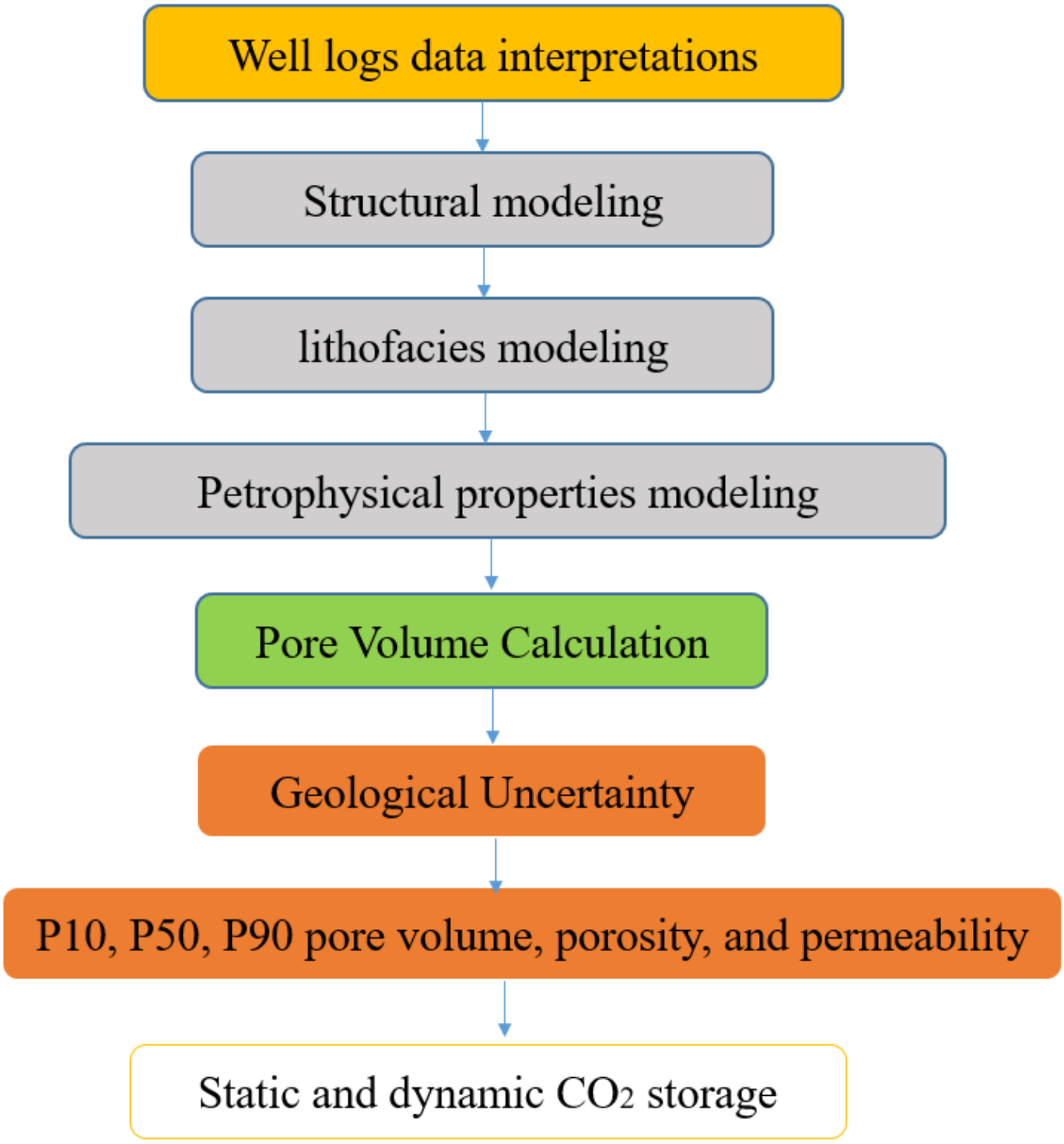

Figure 3

The methodology of static and dynamic CO2 storage in the Sunah oilfield

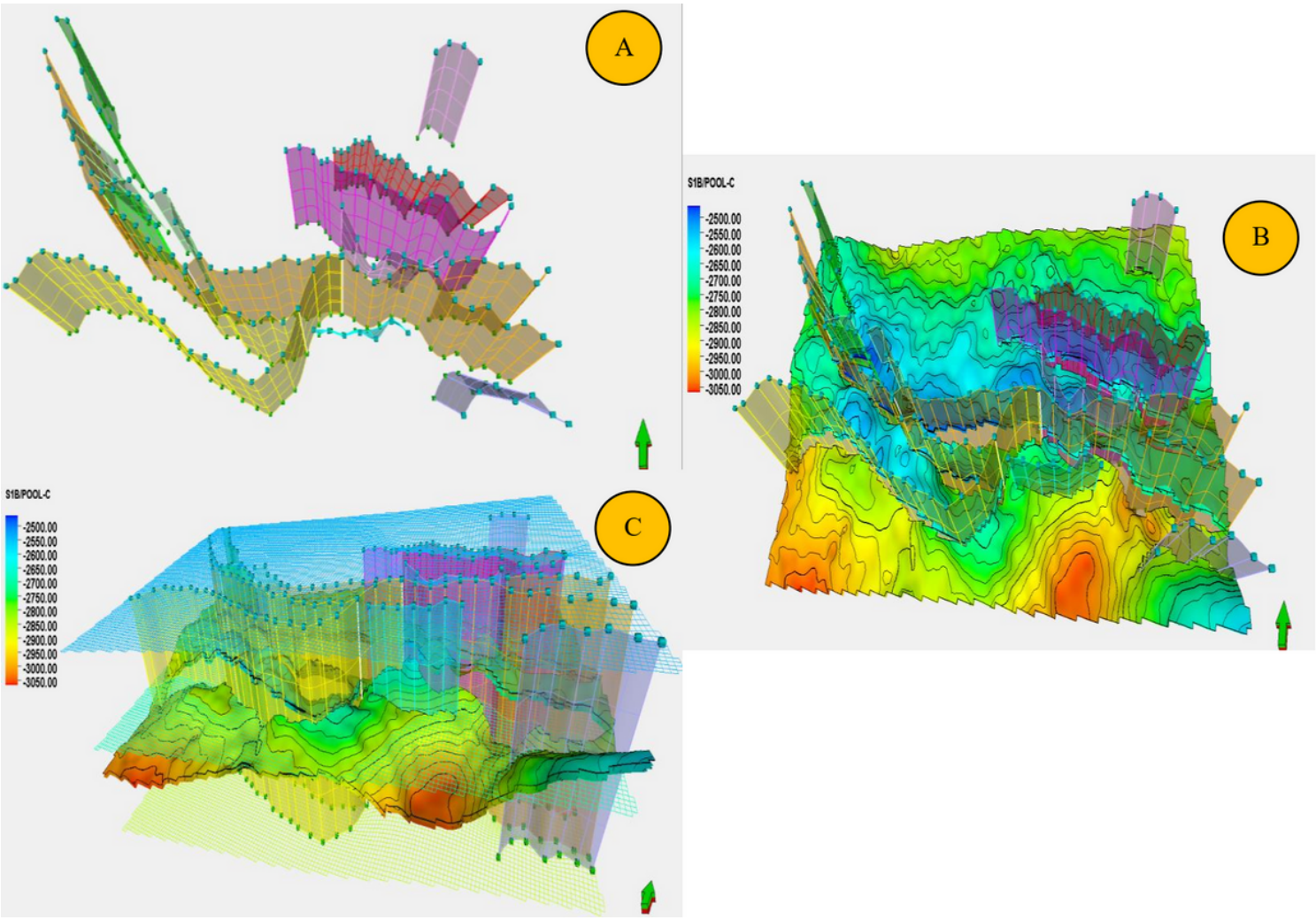

Figure 4

Structural model of S1A. A. fault pillar, B. grid (top, mid, bottom) associated with horizons and fault pillars.C. horizons associated with faults.

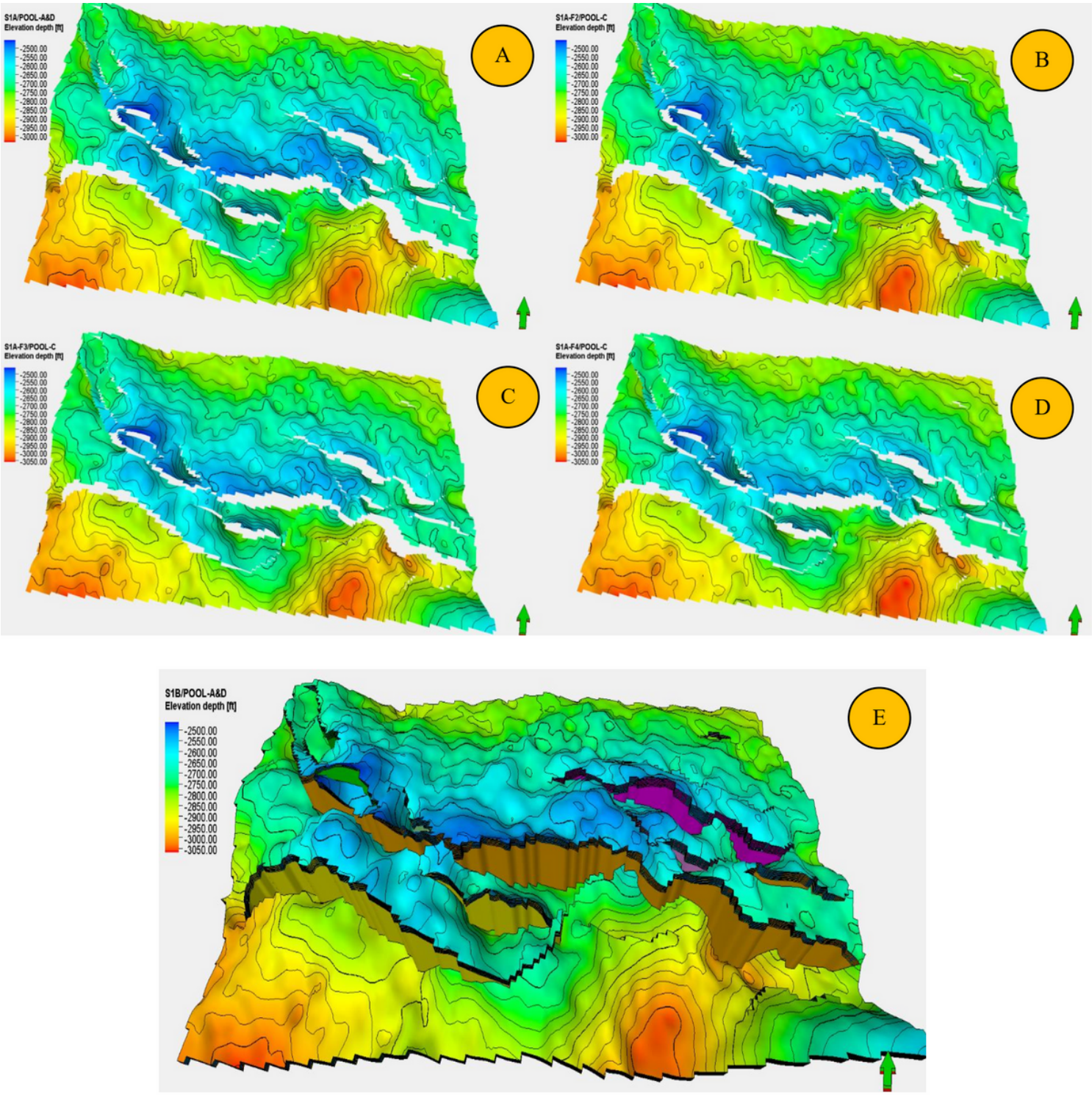

Figure 5

Results of surface modeling in S1A reservoir, Sunah oilfield. A, B, C, and D are the horizons from top to bottom, respectively.

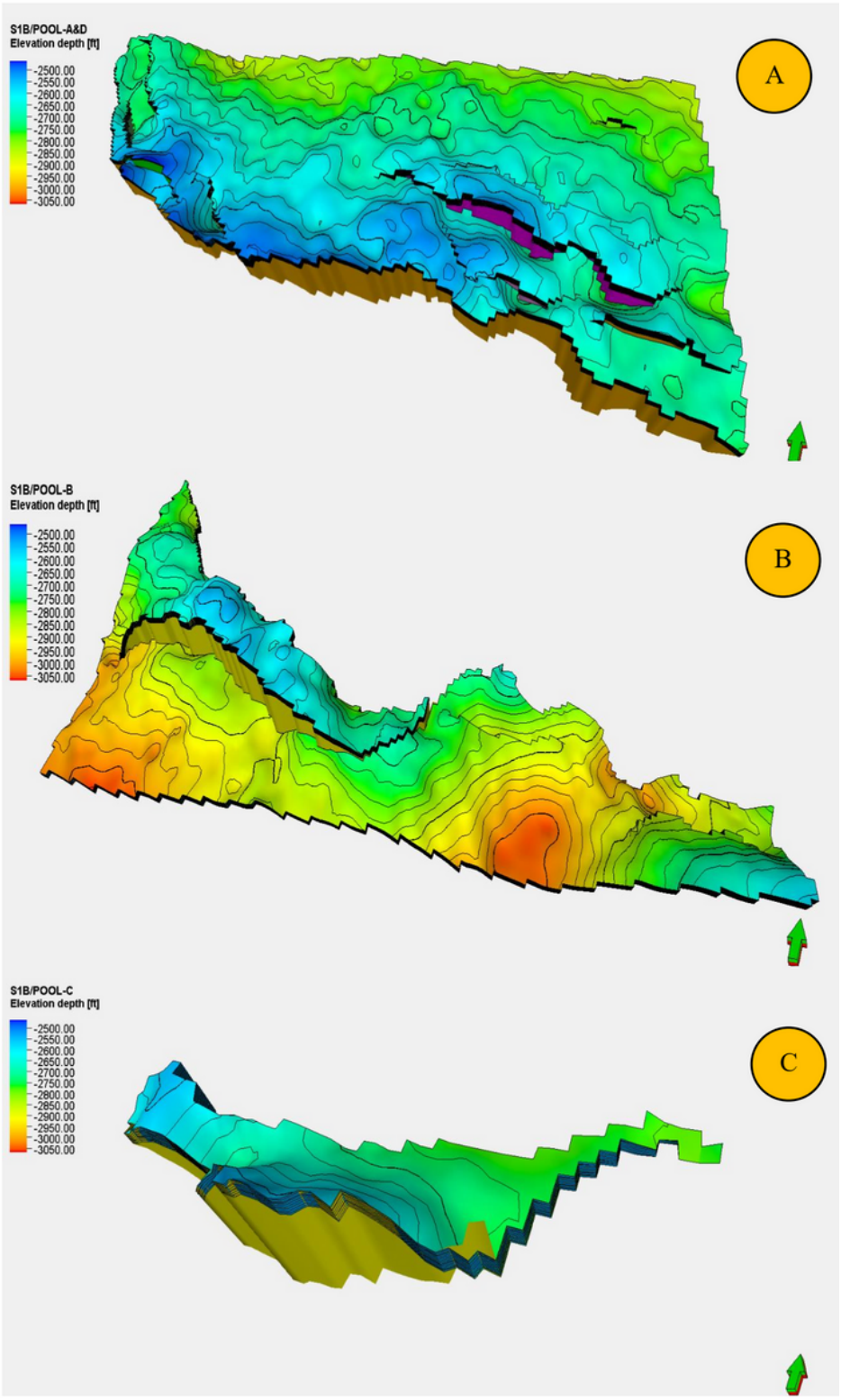

Figure 6

S1A reservoir pool; A. shown the A-D pools; B. shown pool B; C. shown pool C.

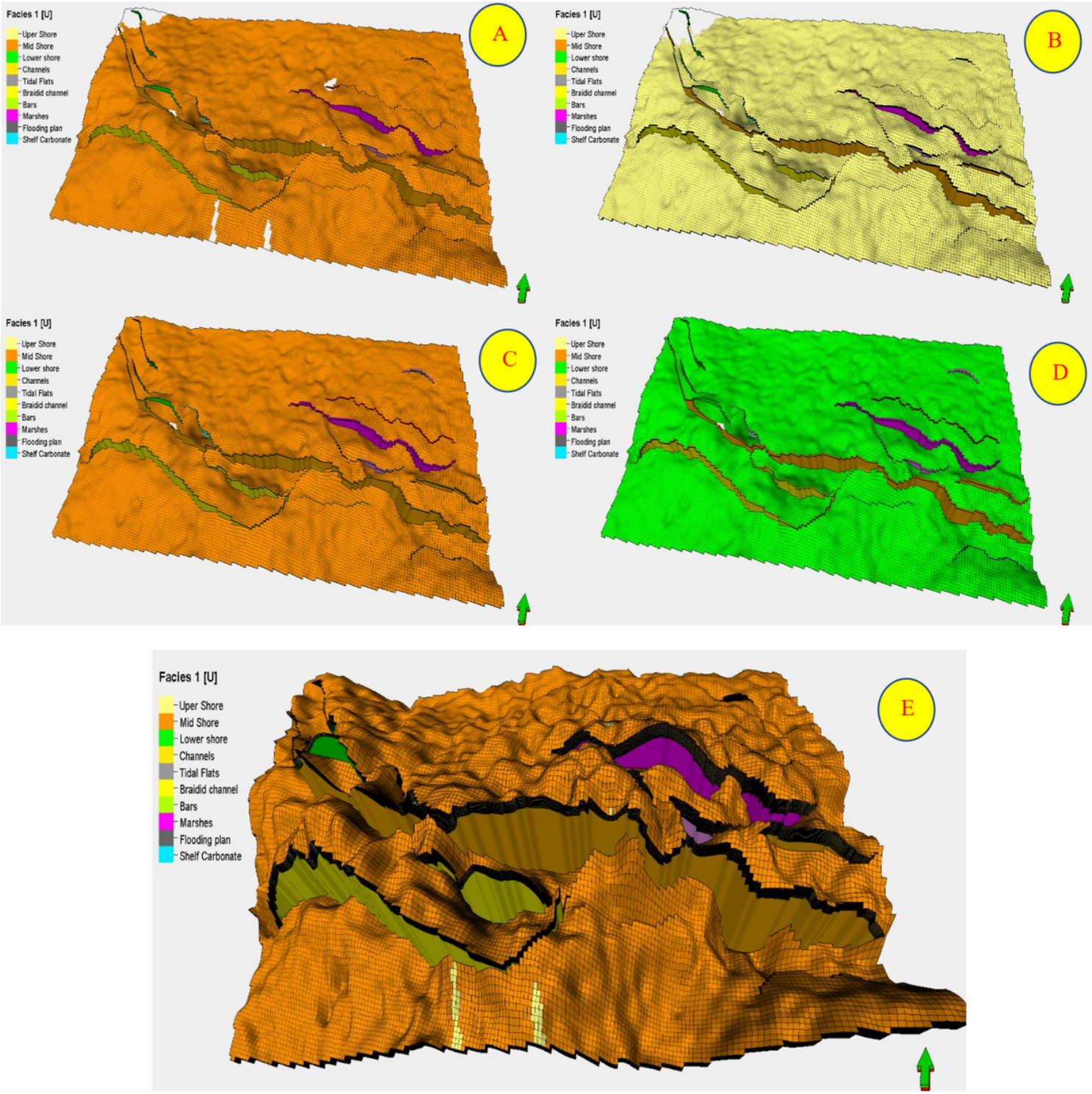

Figure 7

Result of Facies model of S1A reservoir. A, B, C, and D are the reservoir units from top to bottom; consequently, E. facies model of whole S1A reservoir units.

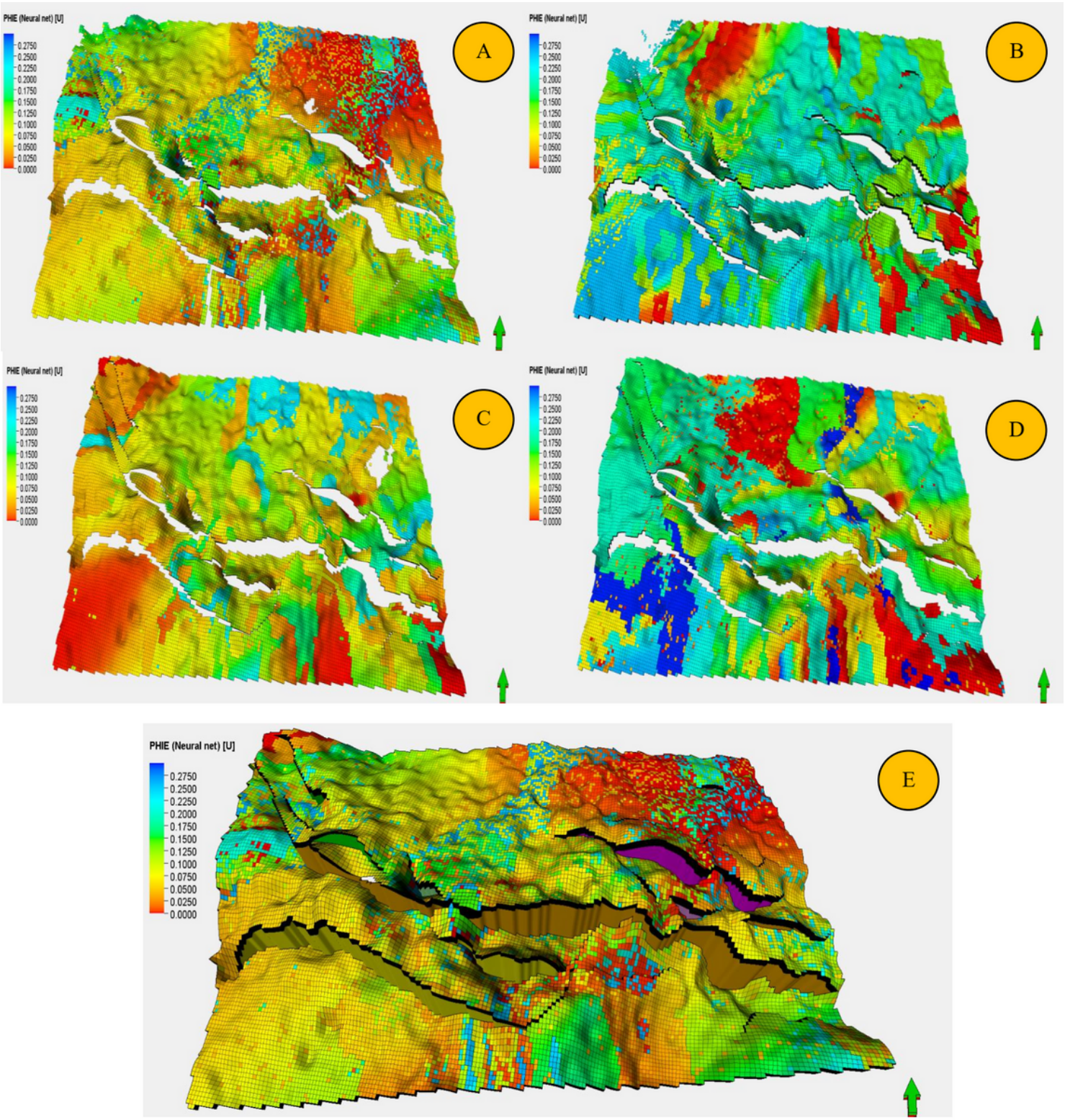

Figure 8

Result of porosity model of the S1A reservoir. A, B, C, and D are the reservoir units from top to bottom. E.porosity model of whole S1A reservoir units

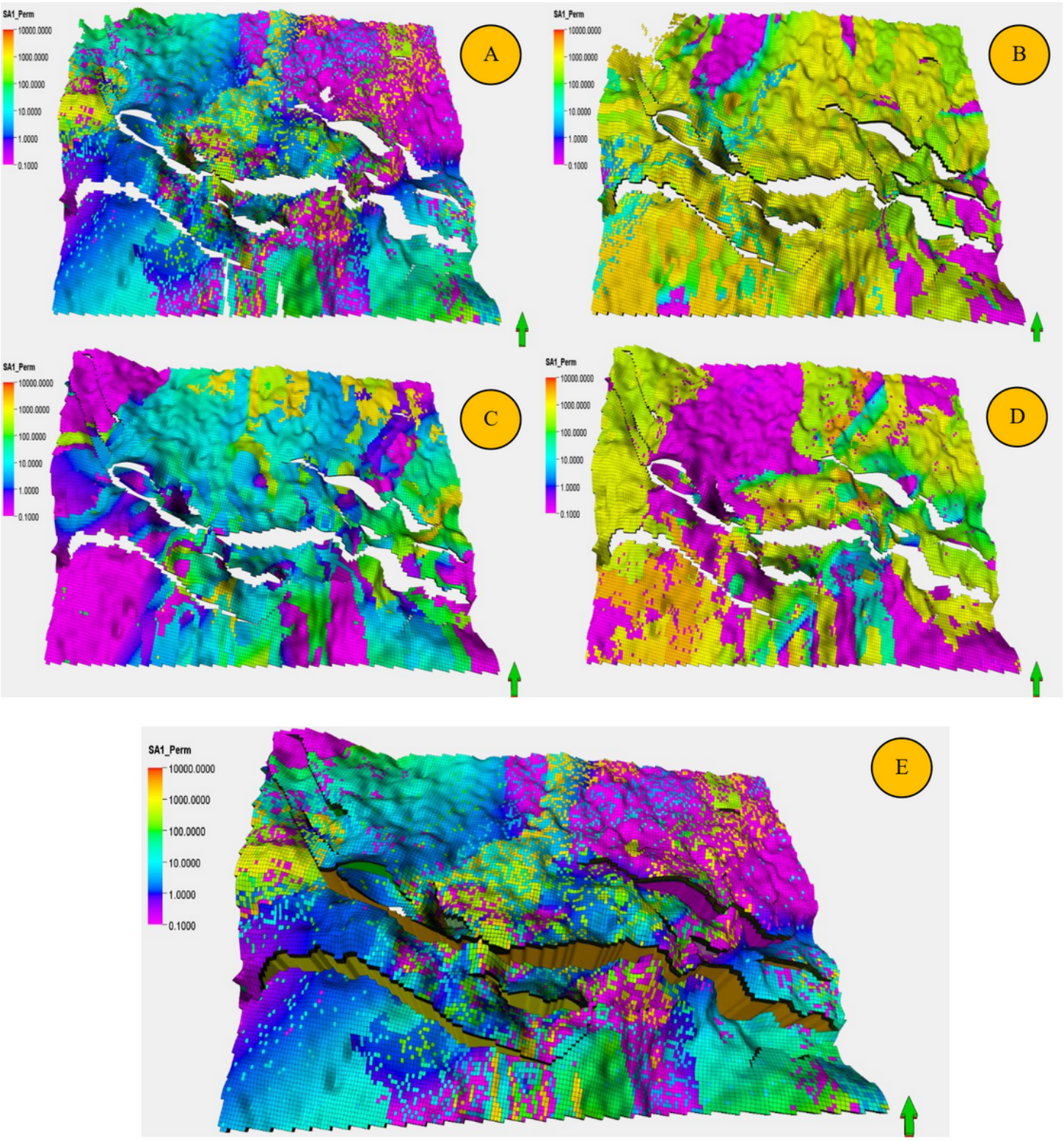

Figure 9

Result of permeability model of S1A reservoir. A, B, C, and D are the permeability reservoir units from top to bottom; consequently, E. permeability model of whole S1A reservoir units

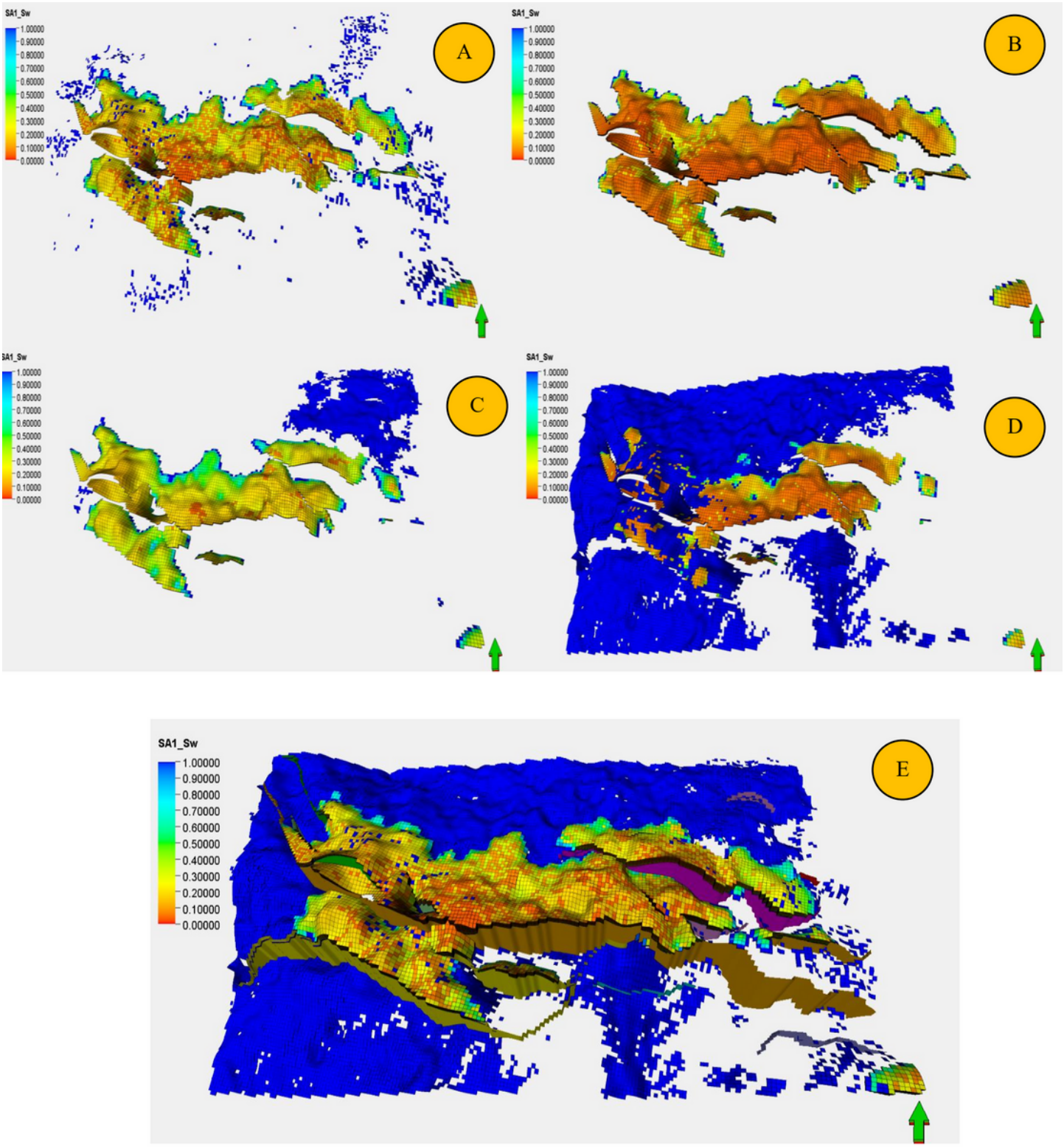

Figure 10

Result of Sw model of S1A reservoir. A, B, C, and D are the water saturation reservoir units from top to bottom consequently, E. Water saturation model of whole S1A reservoir units

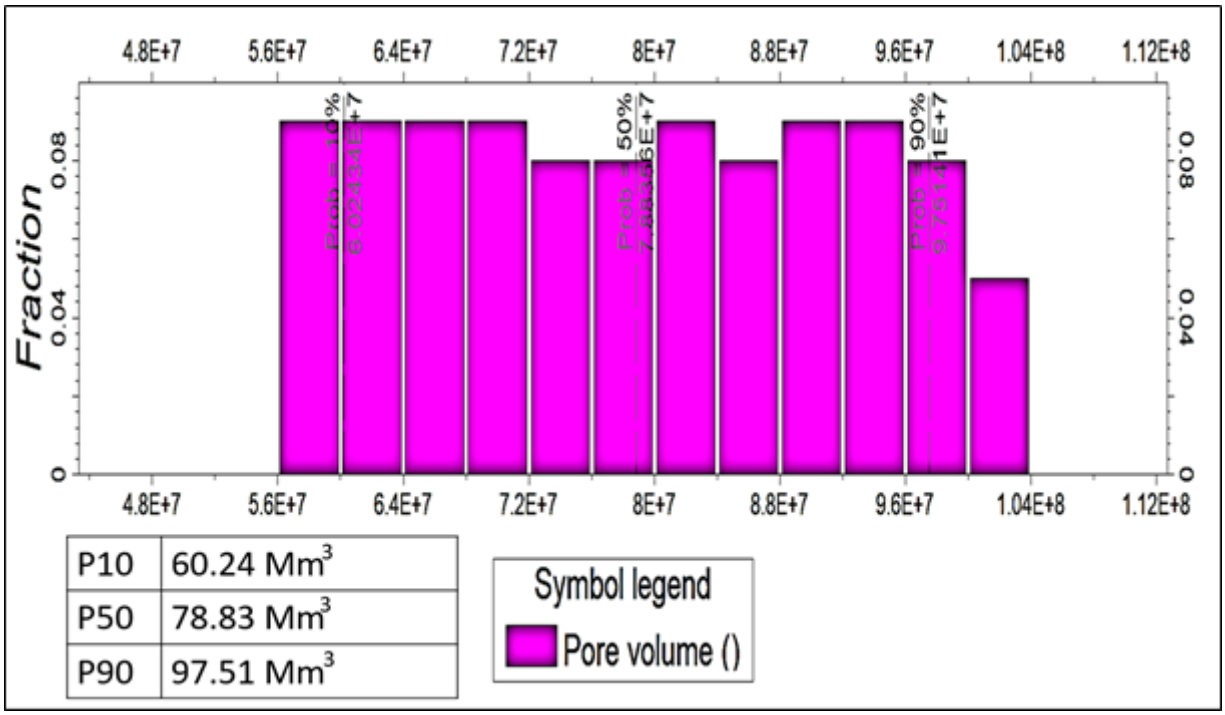

Figure 11

Pore Volume uncertainties for static CO2 storage capacity

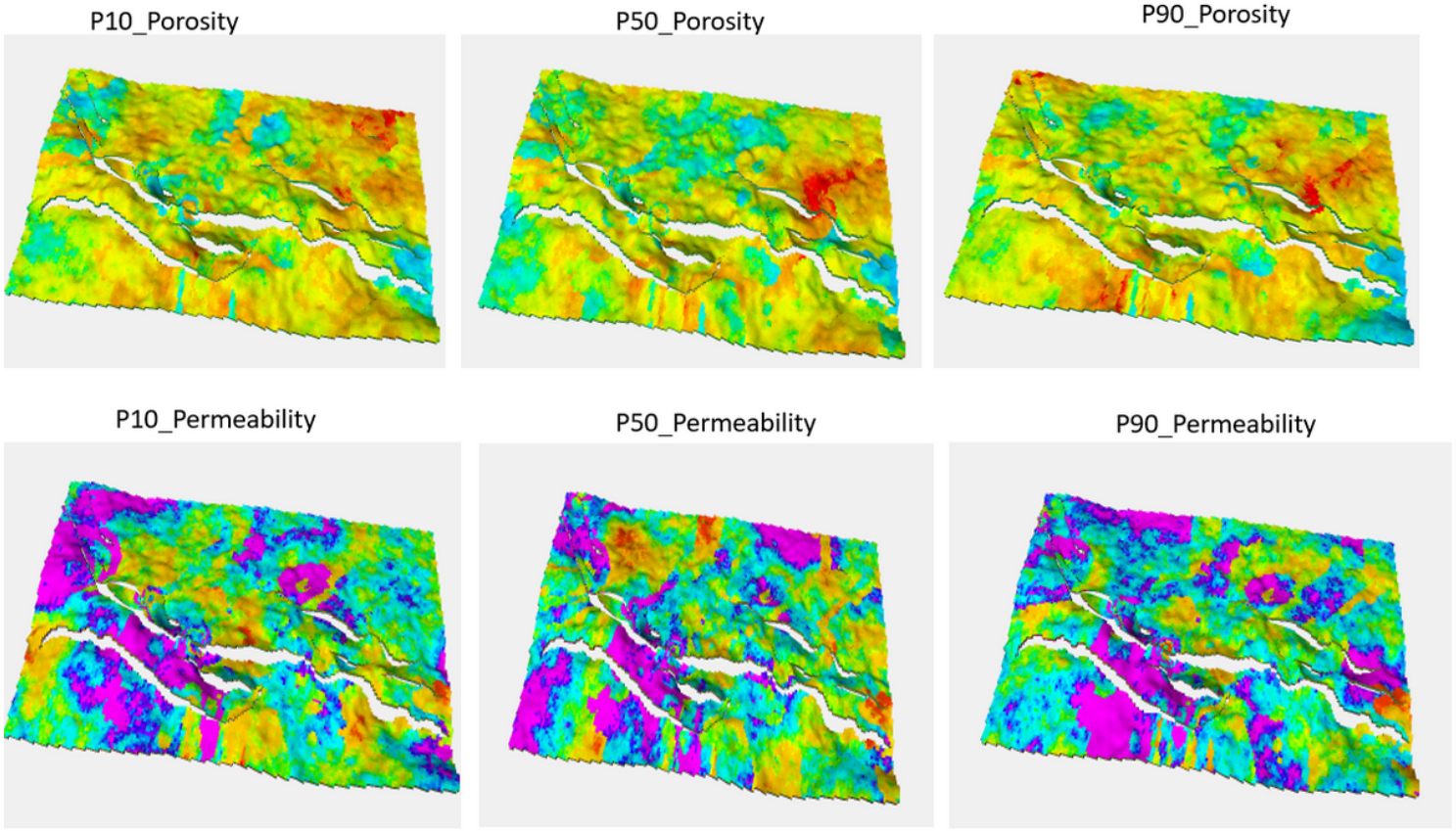

Figure 12

Ranked geological realizations (P10, P50, P90) of porosity and permeability models

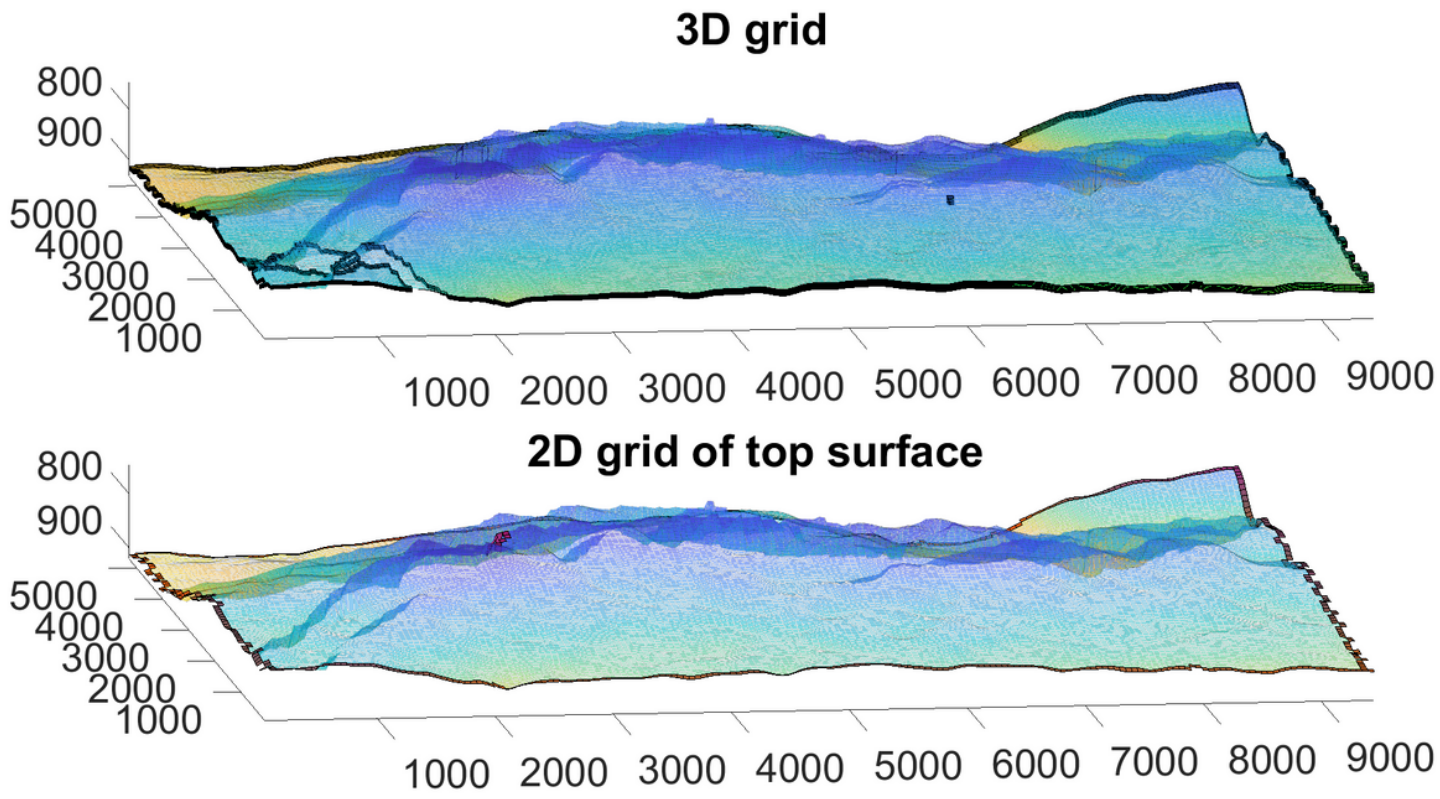

Figure 13

The converting step of VE simulation from 3D domain to 2D model

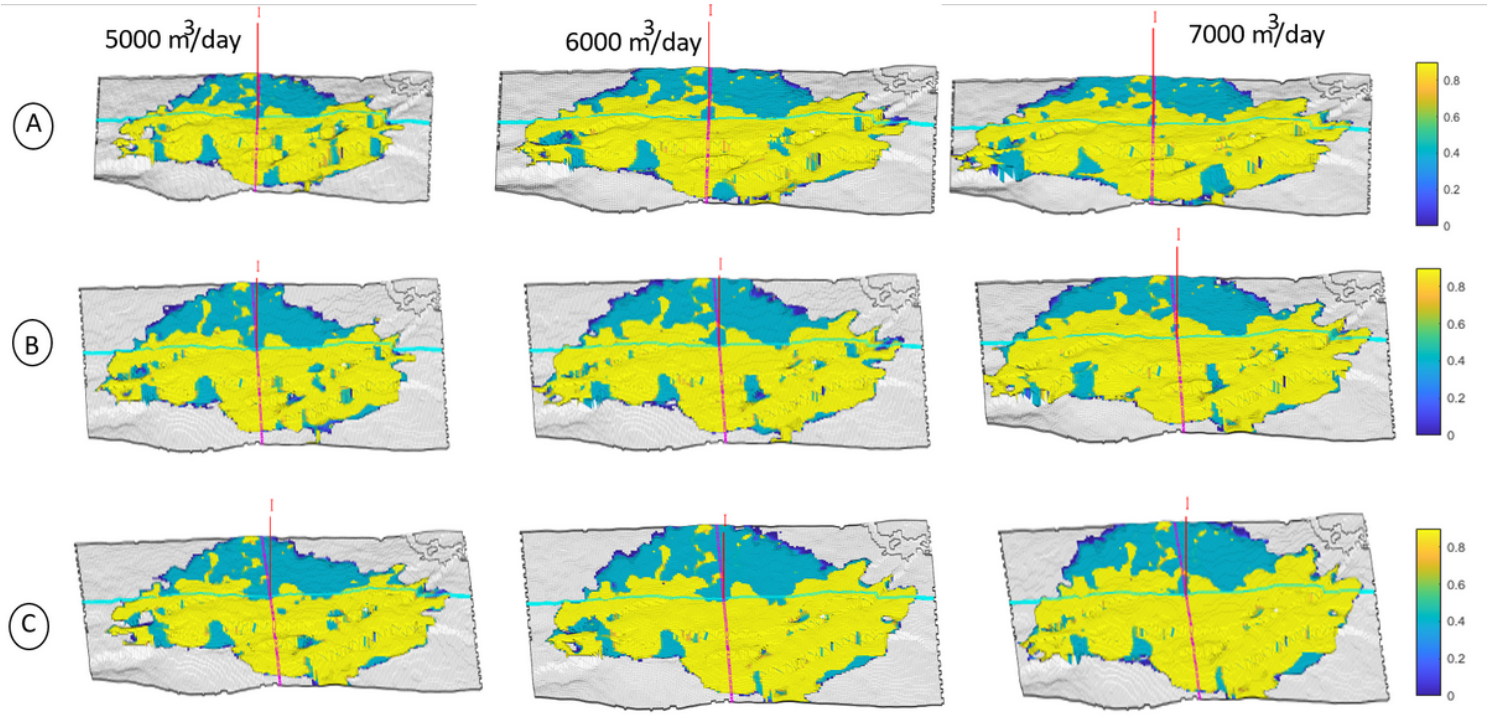

Figure 14

CO2 saturation at 100 years. a.CO2 saturation of P10 geological realization; b. CO2 saturation of P50 realization; c. CO2 saturation of P90 geological realization

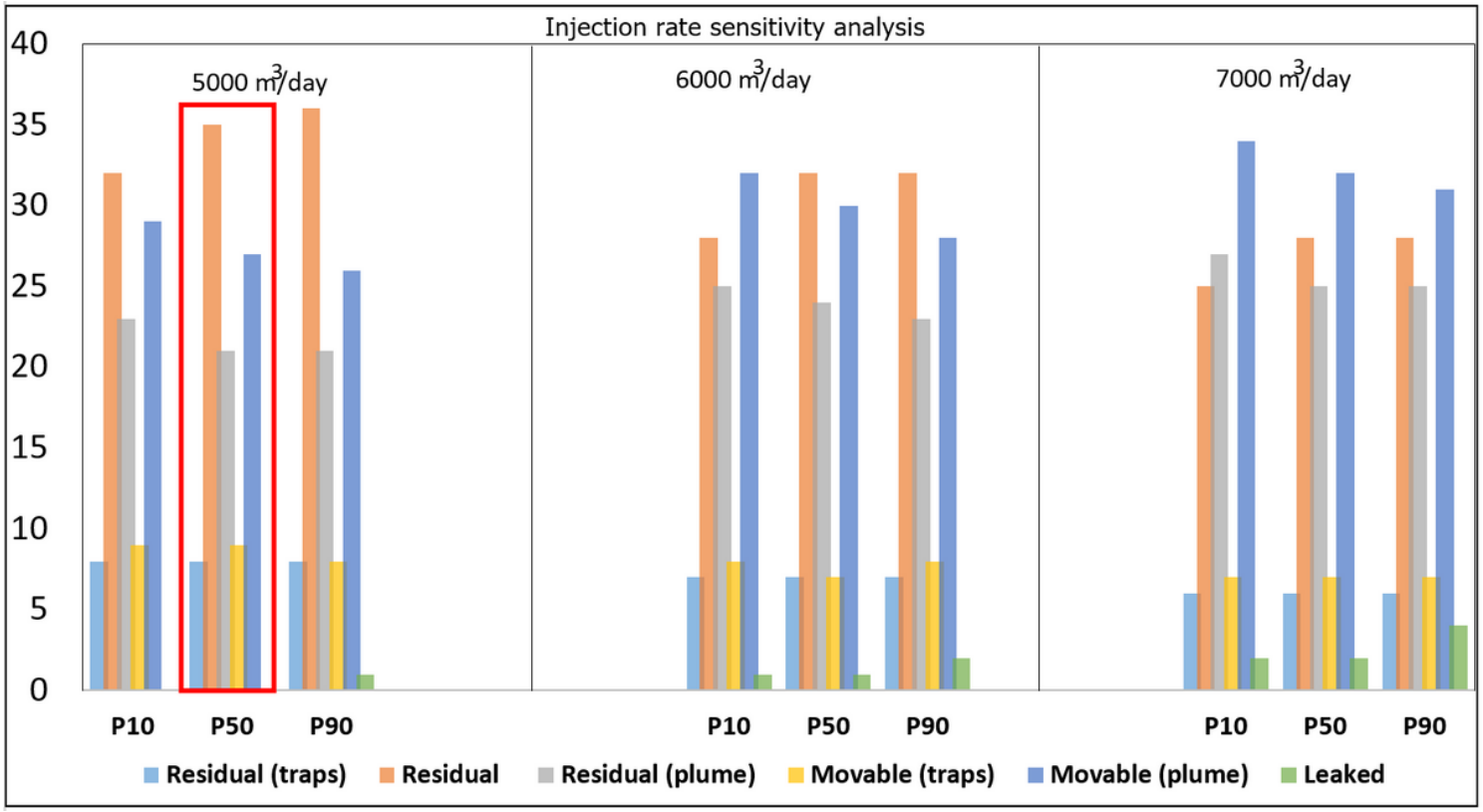

Figure 15

The comparison of three ranked geological realizations with sensitivity injection rate

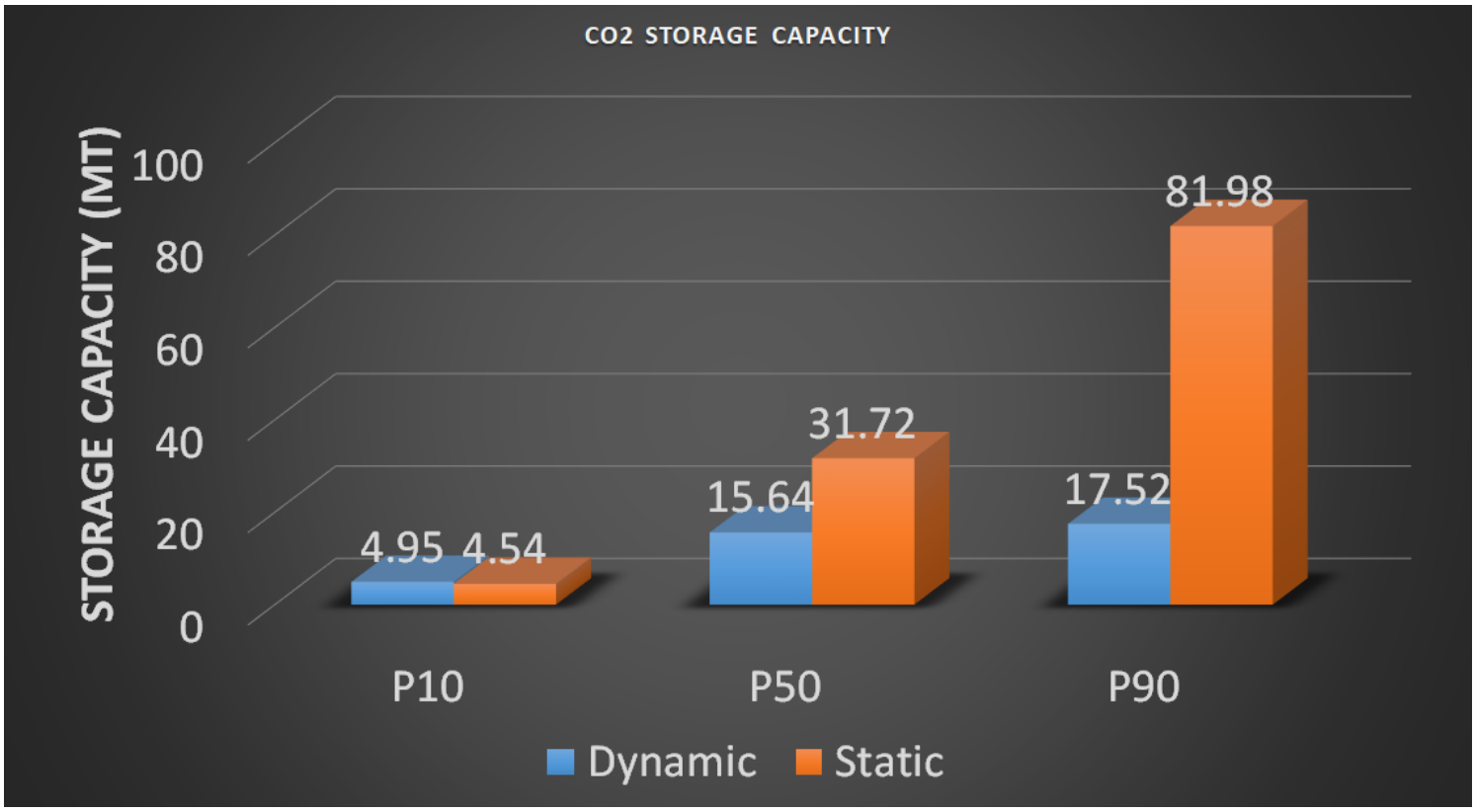

Figure 16

Static and dynamic CO2 storage capacity